Chemical Physics 28 (1978) 253–263

DETERMINATIONS OF BOND ENERGIES BY TIME-OF-FLIGHT SINGLE-COLLISION CHEMILUMINESCENCE

Ron C. ESTLER and Richard N. ZARE
Department of Chemistry, Stanford University, Stanford, California 94305, USA

Received 13 October 1977

A pulsed beam of metastable atoms traverses a scattering chamber filled with oxidant gas at low pressures (beam + gas arrangement); the resulting chemiluminescence is spectroscopically resolved as a function of time to yield a time-of-flight (TOF) spectrum for different internal states. From this data, the initial relative translational energy distribution is derived for the reactants that populate the excited internal state observed. Lower bounds are placed on the barium halide (BaX) dissociation energies, using the reactions $Ba(^3D) + X_2 \rightarrow BaX^* + X$, where X = Br, I. Arguments are presented to show that these lower bounds represent measurements of the true bond energies: it is concluded that $D_0^0(BaBr) = 85.8 \pm 2$ kcal/mole and $D_0^0(BaI) = 72.9 \pm 2$ kcal/mole. The present work corrects previous determinations of bond energies from single-collision chemiluminescent studies which were in error because of unrecognized metastable contamination in the high-temperature atomic beam.

1. Introduction

Bond energies are important quantities in chemistry: they govern the energetics of all chemical reactions. Accurate measurements of bond energies are therefore essential to both the experimentalist and the theorist. Gaydon [1] has reviewed the trandition-al methods of determining bond energies: spectroscopy, thermochemistry, and mass spectrometry. Each technique has its drawback. The Birge–Sponer spectrometric method requires an extrapolation into an unknown regime, thermochemical methods generally suffer from a "weak" link in the thermochemical cycle, and mass spectroscopic methods may be biased due to the internal excitation of the molecule affecting its ionization/fragmentation pattern. In recent years, molecular chemiluminescence under single-collision conditions has also been used to determine bond energies[‡]. It too, has suffered from an inherent uncertainty: the initial relative translational energy of collision partners could only be estimated. We present an improvement of the chemiluminescent method in this paper.

In the past, much of the chemiluminescent work has concentrated on reactions between ground state metal atoms and small polyatomic molecules. It is unfortunate, but unavoidable, that the high-temperature metal atom sources employed in such studies produce a large spread in the initial translational energy E^i_{trans} of the incident beam. Such a thermal energy spread is transformed into an uncertainty in the bond energy.

With the recent interest in the energetics and dynamics of gas-phase reactions of barium with bromine and iodine containing compounds, e.g., Ba + HBr [5], Ba + HI [5,6], Ba + CH_3I [7], Ba + CH_2I_2 [5], Ba + CF_3I [8], Ba + BrCN [9], and Ba + $CH_{4-n}Br_n$, n = 1–4 [10], accurate determinations of the dissociation energies of BaBr and BaI have become increasingly important. To this end, we present here an investigation of the chemiluminescent reactions involving metastable barium atoms, $Ba(^3D)$, with the halogen molecules bromine, Br_2, and iodine, I_2. We describe an apparatus for time-of-flight chemiluminescent studies. Here a pulsed metastable barium beam traverses a scattering chamber filled with oxidant gas at low pressures. A spectrometer views the chemiluminescence at a fixed distance from where the metastable barium atoms are formed. The spectrometer signal as a function of time constitutes the time-of-flight

‡ A partial reference list includes refs. [2–4].

spectrum. We derive from this spectrum the "actual" distribution of E^{i}_{trans}, that is used to set a lower bound to the unknown bond energy.

2. Experimental

The apparatus used in this study, LABSTAR, has been described in detail elsewhere [11]. We note here those modifications made in oven design to produce metastable metal atoms.

The oven assembly consists of a cylindrical graphite heater tube and crucible surrounded by concentric tantalum heat shields. Prior to this investigation, the crucible was positioned inside the heater by a small diameter graphite rod that was connected mechanically and electrically to one end of the heater[‡]. The orifice of the crucible (1 mm dia) was located midway between the ends of the heater tube and directly behind an exit aperture (1 cm dia). In this configuration, however, discharges sporadically occur. The source of this problem appears to be a potential drop between the crucible aperture (at the potential of one end of the heater) and the heater tube exit aperture (at a potential of half the total voltage drop across the entire heater). Such discharges were previously observed in our laboratory with this oven configuration in the study of the $Pb + O_3$ [11] and $Pb + F_2$ [13] chemiluminescent reactions. Barium discharges have also been reported by Haberman [14]★. In addition, it is evident that discharges were present but unrecognized in the study of the $Eu + NO_2$ [15]† and $Ba + I_2$ [16] reactions. The results of these latter two experiments are therefore invalid.

Although there are numerous methods for generating metastable barium [17–20], we have found that a simple modification to the above design appears to be quite efficient. Fig. 1 shows a cutaway view of the oven with these design changes. The crucible is supported from the center of the heater with a cylindrical section of graphite. This assembly forces

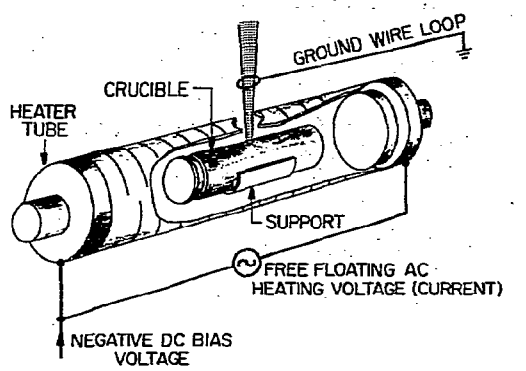

Fig. 1. Pulsed metastable atom source. A few hundred amperes pass through a graphite cylinder, slotted to increase the resistance. A cylindrical section of graphite inside the heater supports a graphite crucible containing the metal sample. This design essentially eliminates potential differences between the crucible and the exit aperture of the heater.

the apertures in the crucible and heater tube to be nearly at the same potential. We place a grounded loop of stainless steel wire (1 mm dia) in close proximity (≈ 3 mm) to the crucible. The ac heating source is free floating and biased negatively with respect to ground by applying a variable dc voltage. The oven operates at a temperature of 1070 K, corresponding to a barium vapor pressure within the crucible of 0.1 torr. A W5%Re/W26%Re thermocouple or an optical pyrometer measures the oven temperature. The voltage–current characteristics of the region between the exit aperture of the oven and the wire loop are similar to those of a glow discharge tube (see, for example, ref. [21]). Once the discharge has been struck, several amperes of current flow through this region.

We did not attempt to detect metastable barium in the voltage range prior to discharge onset. One expects production of the metastable ^3D levels before discharge onset by low energy electron impact excitation through an electron exchange process[‡]. It is well known that singlet–triplet (e.g., $^1S_0 \rightarrow {}^3D$) excitation cross sections peak at impact energies close to threshold (see, e.g., ref. [22]). Detection of these

‡ See fig. 2 of ref. [12].

★ We thank R.B. Bernstein for bringing this reference to our attention.

† The Eu + NO_2 reaction gave a bond energy that was higher than the values determined from the reactions of Eu + N_2O and Eu + O_3; hence, the former determination was used as a lower bound.

‡ Electrons emitted from the heated surfaces are accelerated towards the grounded wire loop inevitably encountering collisions with the Ba atoms whose concentration is high in this region.

levels can be accomplished using laser-induced-fluorescence (LIF) [20] and surface ionization [23]. The $^1D_2$ barium level is also metastable; however, emission studies of barium discharges under beam conditions have shown that over 93% of the metastable population lies in the three fine structure levels of the ^3D term ($^3D_3$, $^3D_2$, $^3D_1$) [18]. Because of this, we limit our discussion of metastable barium to the ^3D levels. Under the operating conditions given above and with no bias voltage, we estimate the flux of ground state Ba($^1S_0$) atoms to be $< 10^{16}$ atoms cm^{-2} s^{-1} in the reaction zone. This oven design also produces controlled discharges of Ca and Sr.

A separately pumped vacuum chamber houses the halogen source and reaction zone. The halogen gas enters the chamber through a small orifice (heated to 100°C for iodine to prevent clogging), while the pressure is regulated outside the chamber using both a constant temperature bath and a teflon stopcock. The halogen beam is uncollimated and it essentially fills the entire reaction chamber (beam + gas arrangement). Single-collision conditions are maintained using low halogen pressures (10^{-5} to 10^{-4} torr).

We use two methods of data collection: analog and digital recording. We describe first the analog configuration. A 1 m f5.6 Interactive Technology spectrometer views the chemiluminescence perpendicular to the metal beam through a quartz window on the reaction chamber. The emission is focussed onto the entrance slit and detected at the exit slit by a cooled Centronic S-20 extended red photomultiplier tube. A picoammeter (Keithley model 417) amplifies the photomultipler current and drives a stripchart recorder.

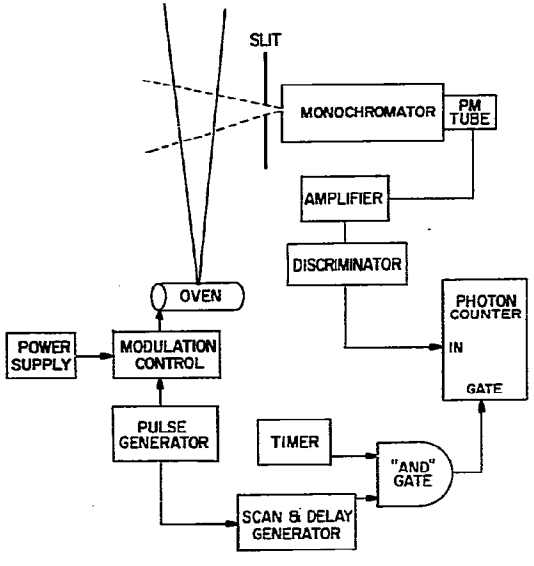

Fig. 2. Schematic of the time-of-flight chemiluminescence detection equipment.

Fig. 2 shows the experimental arrangement for recording digitally the time-of-flight (TOF) dependence of the chemiluminescence. A narrow slit ($\approx$ 2.5 mm) at the reaction zone defines the viewing region and flight path distance L (13.6 cm). Since the excited states of BaBr and BaI are so short-lived ($<$ 18 ns) [24], only chemiluminescence originating from reactive collisions within this region contribute to the TOF signal. We monitor the dependence of the reaction cross section on metastable barium velocity and hence initial translational energy.

A pulse generator (Systron Donner model 100A) provides synchronization for the experiment. At time $t = 0$, a square pulse of width, τ_1, from the generator triggers a negative voltage pulse of the same width from a separate power supply. This negative voltage pulse is applied to the oven (see fig. 1), thereby initiating a discharge and creating metastables. The same timing pulse triggers a scan delay generator (Keithley model 882). At a preset time, T, the flight time, the delay generator puts out a pulse of variable width, τ_2, to provide a gating signal for a counter (Ortec model 772). The pulses from the photomultiplier tube are amplified, discriminated, and counted during the gated observation time, τ_2. The addition of a timer and a logical "and" gate allows counts to accumulate for a preset interval. The timing between $t = 0$ and $t = T$ is calibrated to better than 1% using an oscilloscope (Tektronix model 454), pulse generator and counter.

In practice the spectrometer isolates a particular emission wavelength, while counts accumulate for a 10 s interval at a given flight time. The flight time is then changed randomly to another preset value. The preset flight times were chosen to have a random pattern. Often the measurements were repeated to check for beam stability. For the experiments reported here, the oven is modulated at a rate of 1 kHz with a metastable "on" time (τ_1) of 50 μs and an observation time (τ_2) of 5 μs. Unfortunately, the signal in-

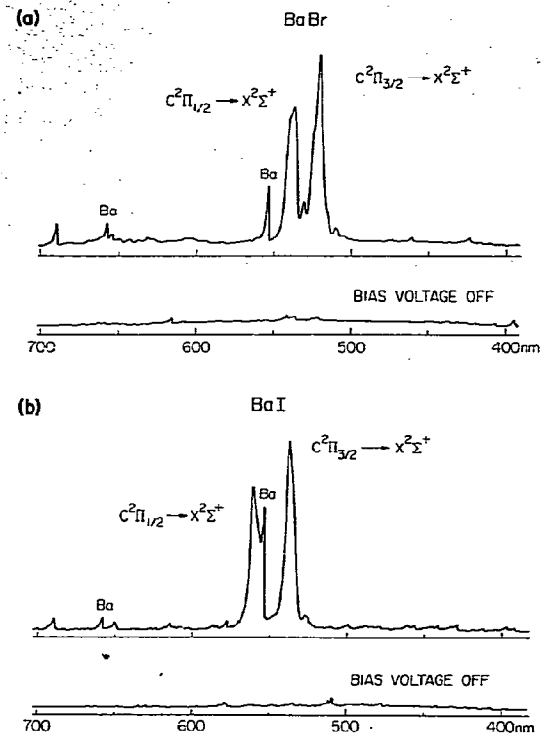

Fig. 3. Low resolution chemiluminescent spectra taken at a scan rate of 50 nm/min and 0.5 nm resolution: (a) Ba (^{3}D) + Br_2; and (b) Ba (^{3}D) + I_2. For comparison, a background spectrum (no Ba excitation) is given for both reactions.

tensities at high optical resolution are too weak to allow the flight time to be set while the emission spectrum is recorded. This procedure provides an alternate method for determining the translational energy dependence of the reaction process[#]. Further discussion of the TOF spectra and analysis is given in section 3.2.

3. Results

3.1. Chemiluminescence spectra and reaction molecularity

Fig. 3 shows the chemiluminescent spectra of the Ba (^{3}D) + Br_2 and Ba (^{3}D) + I_2 reactions, taken at a fast scan rate (50 nm/min) and at low resolution (0.5 nm). Note the on–off behavior of the chemiluminescence with barium excitation. In both spectra the emission originates from the $C\,^2\Pi_{3/2,1/2} \rightarrow X\,^2\Sigma^+$ band system of the corresponding barium halide. The $\Delta v = 0$ sequence dominates both spectra; however, small contributions to the signal from the $\Delta v = 1, -1$ sequences of the $C\,^2\Pi_{3/2} \rightarrow X\,^2\Sigma^+$ system are also evident. In addition, the Ba resonance line at 553.5 nm, as well as other Ba lines are present. Radiation trapping probably causes these atomic lines to appear[‡]. Although not shown in fig. 3, an underlying continuum is present as has been observed previously in other investigations of the Ba + X_2 reactions [26–28].

High resolution spectra (0.1 nm) of the BaBr and BaI $C\,^2\Pi_{3/2} \rightarrow X\,^2\Sigma^+$ systems, taken at a slow scan rate (1 nm/min) are presented in fig. 4. Overlapping of the rotational structure obscures the clarity of the bandheads. BaBr bandhead assignments are based on the work of Cruse et al. [5], BaI bandhead assignments on the work of Patel and Shah [29]. It is necessary to determine the highest vibrational level populated of the metal halide reaction product in order to evaluate the metal halide bond energy. From the spectra shown in fig. 4, as well as others, we find that the $v' = 32$ level of the BaBr $C\,^2\Pi_{3/2}$ state is the highest level populated in the Ba (^{3}D) + Br_2 reaction and the $v' = 40$ level of the BaI $C\,^2\Pi_{3/2}$ state is the highest level in the Ba (^{3}D) + I_2 reaction.

For the bimolecular reaction of metastable barium and a halogen molecule, the chemiluminescence intensity, I, is proportional to the concentration of both, i.e.,

$$I \propto [\mathrm{Ba}(^3\mathrm{D})]\,[\mathrm{X}_2]. \qquad (1)$$

The halogen concentration is proportional to the halogen pressure in the scattering chamber; the metastable barium concentration is proportional to the vapor pressure, P, in the oven, assuming that a con-

[#] A laser-induced-fluorescence experiment has been performed in this manner on the reaction of Al + O_2 by Pasternack and Dagdigian [25] at Johns Hopkins University.

[‡] Radiation trapping in the reaction zone, originating from the discharge region, e.g., $^1P_1^0 \rightarrow {}^1S_0 \rightarrow {}^1P_1^0 \rightarrow {}^1S_0$ (the 553.5 nm transition), raises the possibility that the reaction proceeds through levels other than metastable levels. However, it is unlikely that such processes could produce the concentration of levels required to account for the large cross section reactions observed.

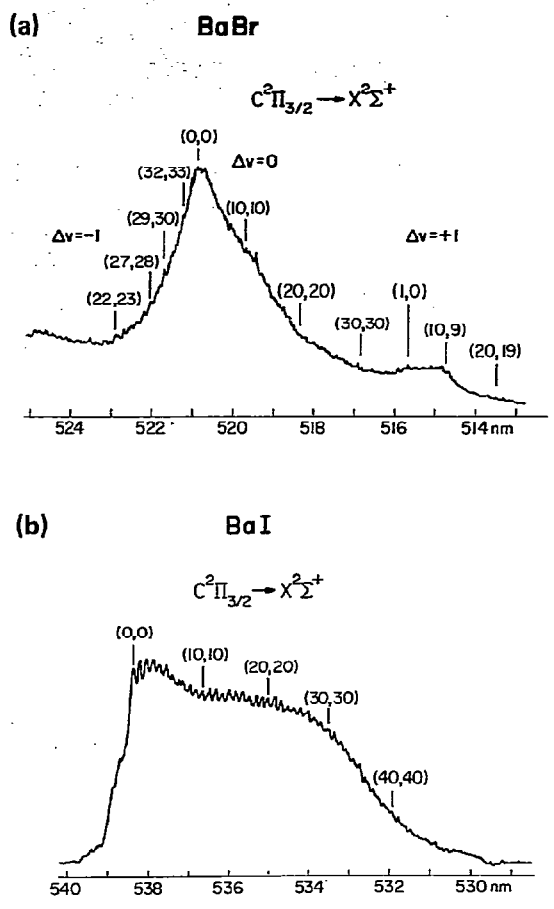

Fig. 4. Higher resolution chemiluminescent spectra taken at a scan rate of 1 nm/min and 0.1 nm resolution: (a) Ba (^{3}D) + Br_2; and (b) Ba (^{3}D) + I_2. For BaBr, the $C^2\Pi_{3/2}-X^2\Sigma^+\Delta v = 0$ and $\Delta v \pm 1$ sequences are shown, while for BaI the $C^2\Pi_{3/2}-X^2\Sigma^+\Delta v = 0$ sequence is shown.

stant fraction of the barium beam is converted by the discharge to metastable barium. With increasing oven temperature, P increases according to the Clausius–Clapeyron equation

$$d\ln P/d(1/T) = -\Delta H_V/R, \qquad (2)$$

where ΔH_V is the latent heat of vaporization at the temperature T. (At the temperature we operate barium is a liquid.) Thus, the reaction molecularity is determined by monitoring the chemiluminescent intensity as a function of halogen pressure and oven temperature.

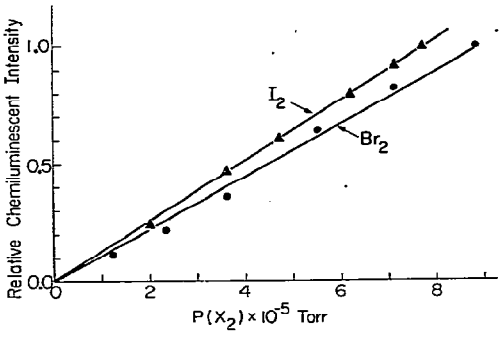

Fig. 5. Plots of the chemiluminescent intensity as a function of halogen pressure at a fixed Ba oven temperature (1070 K). For BaBr, the chemiluminescence was monitored at 520.0 nm and for BaI at 538.0 nm. The linearity of the plots shows that both reactions are first order in halogen concentration.

Figs. 5 and 6 summarize the results of the experiments described above. Both reactions show first order dependence on halogen concentration. Plots of the logarithm of intensity versus the reciprocal of the oven temperature are also linear. The interpretation of the slope of these plots has been investigated by Preuss and Gole [30]. However, they assume a maxwellian distribution of velocities from an effusive source. It is our experience in this study and others [31] that ideal effusive sources are difficult to

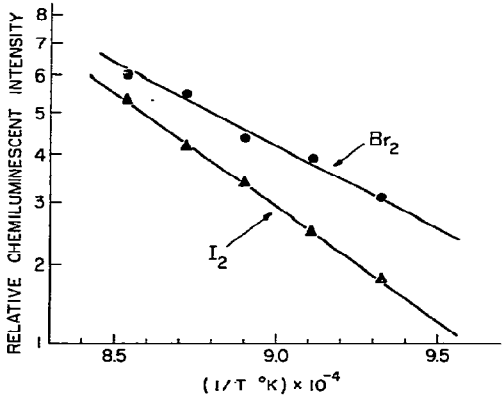

Fig. 6. Plots of the logarithm of the chemiluminescent intentensity as a function of the reciprocal of the absolute temperature at a fixed halogen pressure (1×10^{-4} torr) and a fixed wavelength (520.0 nm for BaBr and 538.0 nm for BaI). The slope and linearity of the plots show that both reactions are first order in Ba (^{3}D) concentration.

achieve. Time-of-flight measurements of metal beams using laser-induced fluorescence support these conclusions [32]. Therefore, we limit our discussion of these plots to their linearity, from which we conclude that the reaction molecularity is first order in metal flux.

Since the reaction is first order in both Ba(^{3}D) and X_2, we conclude that these chemiluminescent reactions proceed via a simple bimolecular mechanism. With the metastable levels of barium having an ionization potential no greater than 4.09 eV‡, one would expect these reactions to take place by a harpoon (electron jump) mechanism [34] as in the case of reactions between alkalies and halogens*. Using the ionization potential given above and the electron affinities of Br_2 and I_2†, the covalent and ionic potential surfaces are calculated to cross at an internuclear separation of 12 Å and 9.8 Å for BaBr and BaI respectively. These crossing radii correspond to very large cross sections: 452 Å for Ba(^{3}D) + Br_2 and 302 Å^2 for Ba(^{3}D) + I_2. However, such large crossing radii indicate a probable breakdown in the electron jump mechanism. Nevertheless, we estimate the cross sections to be 200–300 Å^2. A stripping mechanism where the exothermicity is released early in the approach would account for the high internal excitation of product. No experimental determinations of the cross sections are made.

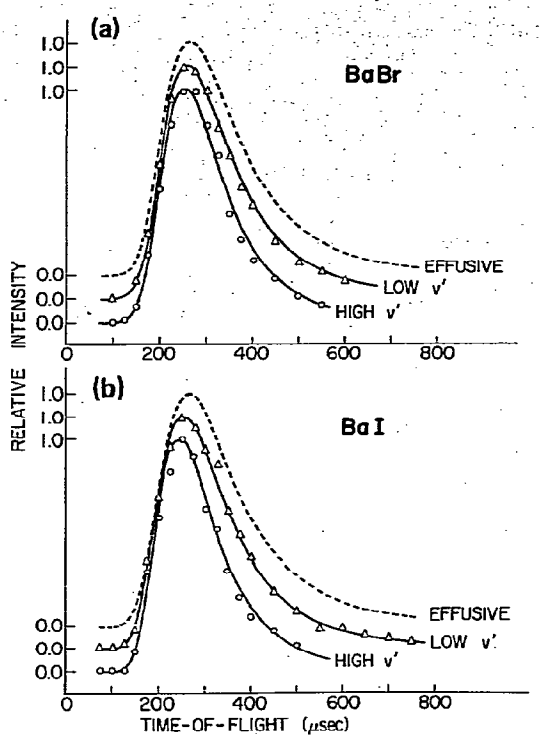

Fig. 7. Time-of-flight spectra: (a) Ba(^{3}D) + Br_2; and (b) Ba(^{3}D) + I_2. The dashed curves are calculated spectra for an effusive Ba source operating at the oven temperature (1070 K).

3.2. TOF spectra and analysis

Fig. 7 shows the chemiluminescence TOF spectra for the BaBr and BaI reactions. In both cases the spectrometer isolates a given portion of the $C\,^2\Pi_{3/2} \rightarrow X\,^2\Sigma^+$ $\Delta v = 0$ sequence with a 1 nm resolution. This resolution is insufficient to observe single (v', v'') transitions. Therefore, these spectra represent the composite signals from several neighboring (v', v'') transitions. The BaBr TOF spectrum for high vibrational levels is centered at 517.5 nm ($v' = 25$), while the one for low vibrational levels is centered at 520.0 nm ($v' = 8$). The 1 nm optical resolution translates into a resolution of ≈ 8 vibrational levels for both BaBr spectra. For BaI, the TOF spectrum of the $v' = 40$ level is monitored at 532.0 nm at a resolution of ≈ 6 vibrational levels and the TOF spectrum of the $v' = 2$ level is monitored at 538.0 nm with the same vibrational level resolution.

The theory of the "single disk" TOF method has been described in detail previously (see for example, refs. [37]). We follow the analysis and nomenclature of Gaily et al. [38]. TOF signals are derived from an assumed gaussian particle flux density

$$I(v) = Nv^3 \exp[-(v-v_0)^2/\sigma_b^2], \qquad (3)$$

where N is a normalization constant and v_0, σ_b are adjustable parameters. Using the experimental variables previously defined, i.e., the flight distance L,

‡ The ground state ionization potential of Ba is 5.21 eV, while the $^3D_3$, $^3D_2$, $^3D_1$ levels lie respectively 1.19 eV, 1.14 eV, and 1.12 eV higher. The upper limit of the metastable ionization potential is therefore, 4.09 eV. See ref. [33].

* A partial reference list includes refs. [35].

† The vertical electron affinities of Br_2 and I_2 are 2.87 eV and 2.6 eV, respectively. See, ref. [36].

the flight time T, the rectangular gate function or beam "on" time τ_1, and the observation time τ_2, the TOF signal is given by

$$F(T) = \int_0^{\tau_1} \mathrm{d}t \int_{v_1(t)}^{v_2(t)} I(v)\,\mathrm{d}v, \tag{4}$$

where the limits of the second integral are

$$v_1(t) = L/(T + \tau_2 - t), \tag{5}$$

and

$$v_2(t) = L/(T - t). \tag{6}$$

The v_0 and σ_b parameters are determined by fitting the observed TOF spectra to simulated TOF spectra. This fitting procedure is not a least squares analysis: instead, we match peak intensities and halfwidths. Fig. 7 also presents the generated TOF spectra for an effusive source at the oven operating temperature. Table 1 summarizes the values of v_0 and σ_b used to make these fits. No correction is made in the analysis for the decay of the metastables during the flight time. Since the ^{3}D levels have lifetimes > 1 ms [23], we do not consider this a serious omission.

In table 1, the higher vibrational levels of product corresponds to distributions centered about higher values of v_0. Since v_0 is a measure of the relative translational energy prior to collision, it is not surprising to find this correlation.

Table 1
TOF parameters in units of 10^4 cm/s for $I(v) = Nv^3 \times \exp[-(v-v_0)^2/\sigma_b^2]$

	v'	Resolution	v_0 a)	σ_b b)
BaBr	8	≈ 8	0.75	3.43
	25	≈ 8	2.30	2.96
BaI	2	≈ 6	0.50	3.60
	40	≈ 6	2.20	3.16

a) Estimated uncertainty of ± 20%.
b) Estimated uncertainty of ± 10%.

4. BaBr and BaI bond energies

The accurate determination of the bond energies of BaBr and BaI has eluded investigators for many years. Table 2 summarizes all known previous determinations. Generally, the values for each molecule fall into two groups with 15–20 kcal/mole separating the respective averages. Previous chemiluminescent determinations [16,39] appear to have suffered from metastable barium contamination in the beam since these values are in disagreement with the others by an amount approximately equal to the metastable excitation energy.

In the present experiment, we consider the following reactions:

Table 2
Determinations of BaBr and BaI dissociation energies

Molecule	Investigator	Method	D_0^0 (kcal/mole)
BaBr	Krasnov and Karaseva [45]	ionic model calculation	100 ± 15
	Gole [46]	chemiluminescence	⩾ 99
	Gurvich et al. [47]	flame spectroscopy	87.5 ± 2.0
	Menzinger [39]	chemiluminescence	104.6 ± 2
	Hildenbrand [42]	mass spectrometry	85.5 ± 2.2
	Estler and Zare (this work)	chemiluminescence	85.8 ± 2
BaI	Krasnov and Karaseva [45]	ionic model calculation	85 ± 15
	Mims et al. [6]	molecular beam scattering	⩾ 66
	Gole [46]	chemiluminescence	⩾ 97
	Dickson et al. [16]	chemiluminescence	102 ± 1
	Hildenbrand [43]	mass spectrometry	71.4 ± 1.0
	Estler and Zare (this work)	chemiluminescence	72.9 ± 2

$$Ba(^3D) + Br_2(X\,^1\Sigma_g^+) \rightarrow BaBr(C\,^2\Pi_{3/2}) + Br(^2P^o_{3/2}),$$

and

$$Ba(^3D) + I_2(X\,^1\Sigma_g^+) \rightarrow BaI(C\,^2\Pi_{3/2}) + I(^2P^o_{3/2}).$$

The dissociation energy for the barium halide molecule, $D_0^0(BaX)$, is defined as the energy required to separate the molecule in the lowest (v, J) energy level of the ground electronic state into constituent atoms in their lowest energy states. Thus, by applying energy balance to the reactions given above, we obtain the equality

$$D_0^0(BaX) = D_0^0(X_2) + E_{int}(BaX) + E^f_{trans} - E_{int}(Ba) - E_{int}(X_2) - E^i_{trans}, \quad (7)$$

where $E_{int}(BaX)$, $E_{int}(Ba)$, and $E_{int}(X_2)$ are the internal energies of the barium halide, the barium atom, and the halogen molecule respectively, and E^i_{trans} and E^f_{trans} are the initial and final relative translational energies, measured in the center-of-mass frame. Because we measure the highest internal energy state of the metal halide, it is important to understand that E^i_{trans} and E^f_{trans} are not the average values of the relative translational energy before and after collision, but refer to the relative translational energy of collision partners leading to the population of this product state. We have not determined E^f_{trans} in this experiment. The neglect of this term in eq. (7) does not markedly affect the final determination, since we believe that the E^f_{trans} corresponding to the highest internal energy of product is nearly zero. This assumption is based in addition on the fact that the early downhill approach of the expected potential surface channels most of the exothermicity into the internal excitation of product rather than into post-collision relative translational energy [40]. Therefore, the omission of this term gives

$$D_0^0(BaX) \geq D_0^0(X_2) + E_{int}(BaX) - E_{int}(Ba) - E_{int}(X_2) - E^i_{trans}. \quad (8)$$

This inequality provides a lower bound to the barium halide dissociation energy: moreover, we expect this lower bound to be an excellent approximation to the true value.

4.1. Relative translational energy distributions

Dagdigian et al. [41], have derived the initial relative translational energy distribution for collision partners in a beam + gas arrangement. We extend their derivation to include a beam characterized by eq. (3) (see the appendix).

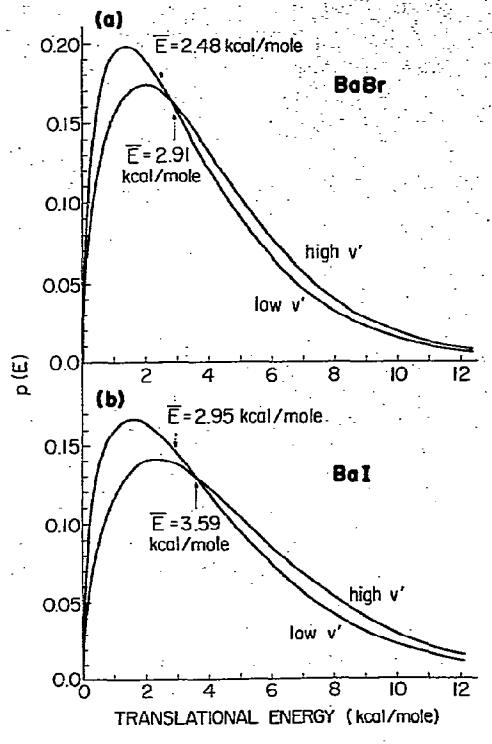

Fig. 8. Initial relative translational energy distributions for a "beam-gas" arrangement derived from the TOF spectra given in fig. 7; distributions for high and low vibrational levels (a) of the BaBr product and (b) of the BaI product. The average energy $\bar{E}$ is marked for each distribution.

Fig. 8 shows the resulting translational energy distributions. In each case, we evaluate the average energy, $\bar{E}$, numerically. The distributions are very wide: yet, the expected trend is apparent. The average translational energy is greater for higher BaX vibrational levels. The large spread in the distributions becomes the main source of error in determining $D_0^0(BaX)$ from eq. (8). In the past, E^i_{trans} has been estimated either assuming a head-on collision of reactants with their most probable velocities [3] or using a mass weighted effective temperature [16] with,

$$E^i_{trans} = \tfrac{3}{2} k T_{eff}, \quad (9)$$

where, for example,

$$T_{\mathrm{eff}} = [T(\mathrm{Ba})\, m(\mathrm{X_2}) + T(\mathrm{X_2})\, m(\mathrm{Ba})] \times [m(\mathrm{X_2}) + m(\mathrm{Ba})]^{-1}. \quad (10)$$

We have equated $E^{\mathrm{i}}_{\mathrm{trans}}$ with the value of $\bar{E}$ for the high vibrational energy distributions. This is much more satisfying since these distributions, within the context of our velocity model [eq. (3)], represent the relative translational energy distributions for the highest internal states observed.

4.2. Calculation of the dissociation energies

The values of the terms in eq. (8) are listed in table 3 for both BaBr and BaI. Where appropriate, the various terms are evaluated using spectroscopic constants for the particular species. We find

Table 3
Energies (kcal/mole) used to calculate lower bound to $D^0_0(\mathrm{BaX})$

	BaBr	BaI
$D^0_0(\mathrm{Br_2})$	45.44 a)	–
$D^0_0(\mathrm{I_2})$	–	35.57 b)
$E_{\mathrm{int}}(\mathrm{BaX})$	72.00	69.90
$E_{\mathrm{int}}(\mathrm{Ba})$	27.44 c)	27.44 c)
$E_{\mathrm{int}}(\mathrm{X_2})$	1.30 total 0.59 rotation d) 0.71 vibration e)	1.51 total 0.74 rotation d) 0.77 vibration e)
$E^{\mathrm{i}}_{\mathrm{trans}}(\bar{E})$	2.91	3.59

a) Ref. [48]. b) Ref. [49].
c) The $^3D_3$ Ba level (highest energy fine structure component) has been used to provide a lower limit.
d) RT, where $T = 300$ K for Br_2 and $T = 373$ K for I_2.
e) Average value calculated using spectroscopic constants: for Br_2, see ref. [50], and for I_2, see ref. [48].

$$D^0_0(\mathrm{BaBr}) = 85.8 \pm 2 \text{ kcal/mole}, \quad (11)$$

and

$$D^0_0(\mathrm{BaI}) = 72.9 \pm 2 \text{ kcal/mole}. \quad (12)$$

We place an uncertainty of ± 2 kcal/mole on the dissociation energies since the distributions of initial translational energy are so broad. The combined uncertainties of all the other quantities appearing in eq. (8) are less than ± 2 kcal/mole. These dissociation energies are in good agreement with those recently measured by Hildenbrand using mass spectrometric techniques [42,43].

5. Conclusions

We have determined the dissociation energies, $D^0_0(\mathrm{BaBr})$ and $D^0_0(\mathrm{BaI})$, to be 85.8 ± 2 kcal/mole and 72.9 ± 2 kcal/mole, respectively, using the technique of time-of-flight single-collision chemiluminescence. We believe the methods employed in the present study will prove valuable in future bond energy determinations as well as in the investigations of the dynamics of chemiluminescent reactions.

Acknowledgement

We are grateful to P.J. Dagdigian, D.L. Hildenbrand, and L. Pasternack for making their results available to us prior to publication. We also thank the US Army Research Office for their support. This work was started at Columbia University under Grant No. DAAG 29-76-G-0208 and completed at Stanford University under Grant No. DAG-29-77-G-0151.

Appendix: Initial relative translational energy distribution

We have extended the derivation of Dagdigian et al. [41] for a beam characterized by eq. (3). Analogous to ref. [41], we define the velocity density distributions of the collision partners as

$$f(v_{\mathrm{b}})\, \mathrm{d}v_{\mathrm{b}} = 4 N v_{\mathrm{b}}^2 \sigma_{\mathrm{b}}^{-3} \pi^{-1/2} \exp[-(v - v_0)^2/\sigma_{\mathrm{b}}^2]\, \mathrm{d}v_{\mathrm{b}} \quad \text{(beam)}, \quad (A1)$$

and

$$f(v_{\mathrm{g}})\, \mathrm{d}v_{\mathrm{g}} = v_{\mathrm{g}}^2 \sigma_{\mathrm{g}}^{-3} \pi^{-3/2} \exp(-v_{\mathrm{g}}^2/\sigma_{\mathrm{g}}^2)\, \mathrm{d}v_{\mathrm{g}} \quad \text{(gas)}. \quad (A2)$$

The beam parameters v_0 and σ_b are experimentally determined and

$$\sigma_g = [2kT(X_2)/m(X_2)]^{1/2}. \tag{A3}$$

N is a normalization constant. Carrying out an analysis similar to that in ref. [41] [through eq. (A8)], we obtain the squared relative velocity distribution,

$$P(v_r^2) = N(2\sigma_g\pi^{1/2})^{-1}\exp(-v_r^2/\sigma_g^2)\exp(-v_0^2/\sigma_b^2)$$
$$\times\left\{\int_0^\infty v_b \exp\left[-\left(\frac{1}{\sigma_g^2}+\frac{1}{\sigma_b^2}\right)v_b^2 - 2\left(\frac{-v_r}{\sigma_g^2}-\frac{v_0}{\sigma_b^2}\right)v_b\right]dv_b - \int_0^\infty v_b \exp\left[-\left(\frac{1}{\sigma_g^2}+\frac{1}{\sigma_b^2}\right)v_b^2 - 2\left(\frac{v_r}{\sigma_g^2}-\frac{v_0}{\sigma_b^2}\right)v_b\right]dv_b\right\}. \tag{A4}$$

The two nearly identical integrals within the brackets are recognized as tabulated [44]. The final result is given by

$$P(v_r^2) = N(2\sigma_g\pi^{1/2})^{-1}\exp(-v_r^2/\sigma_g^2)\exp(v_0^2/\sigma_b^2)$$
$$\times\left\{\left[\frac{1}{2\alpha}-\frac{\gamma_1}{2\alpha}(\pi/\alpha)^{1/2}\exp(\gamma_1^2/\alpha)[1-\mathrm{erf}(\gamma_1/\alpha^{-1/2})]\right]-\left[\frac{1}{2\alpha}-\frac{\gamma_2}{2\alpha}(\pi/\alpha)^{1/2}\exp(\gamma_2^2/\alpha)[1-\mathrm{erf}(\gamma_2/\alpha^{-1/2})]\right]\right\}, \tag{A5}$$

where

$$\alpha = \left(\frac{1}{\sigma_g^2}+\frac{1}{\sigma_b^2}\right), \quad \gamma_1 = \left(\frac{-v_r}{\sigma_g^2}-\frac{v_0}{\sigma_b^2}\right), \quad \gamma_2 = \left(\frac{v_r}{\sigma_g^2}-\frac{v_0}{\sigma_b^2}\right). \tag{A6}$$

This expression is related to the initial relative energy probability distribution by

$$p(E) = (2/\mu)v_r^2, \tag{A7}$$

where μ is the reduced mass of the collision partners. We use (A5) and (A7) to plot the translational energy distributions shown in fig. 8.

References

[1] A.G. Gaydon, Dissociation energies and spectra of diatomic molecules (Chapman and Hall, London, 1968).

[2] Ch. Ottinger and R.N. Zare, Chem. Phys. Letters 5 (1970) 243;
C.D. Jonah, R.N. Zare and Ch. Ottinger, J. Chem. Phys. 56 (1972) 263;
J.L. Gole and R.N. Zare, J. Chem. Phys. 57 (1972) 5331.

[3] R.N. Zare, Ber. Bunsenges. Phys. Chem. 78 (1974) 153.

[4] F. Engelke, R.K. Sander and R.N. Zare, J. Chem. Phys. 65 (1976) 1146.

[5] H.W. Cruse, P.J. Dagdigian and R.N. Zare, Faraday Discussions Chem. Soc. 55 (1973) 277.

[6] C.A. Mims, S.-M. Lin and R. Herm, J. Chem. Phys. 57 (1972) 3099.

[7] P.J. Dagdigian, H.W. Cruse and R.N. Zare, Chem. Phys. 15 (1976) 249.

[8] G.P. Smith, J.C. Whitehead and R.N. Zare, J. Chem. Phys. 67 (1977) 4912.

[9] L. Pasternack and P.J. Dagdigian, J. Chem. Phys. 65 (1976) 1320.

[10] M. Rommel and A. Schultz, Ber. Bunsenges. Physik. Chem. 81 (1977) 139.

[11] R.C. Oldenborg, C.R. Dickson and R.N. Zare, J. Mol. Spectry. 58 (1975) 283.

[12] C.R. Dickson, S.M. George and R.N. Zare, J. Chem. Phys. 67 (1977) 1024.

[13] C.R. Dickson and R.N. Zare, Optica Pura y Aplicada, to be published.

[14] J.A. Haberman, Ph.D. Thesis, University of Wisconsin (1975) p. 492.

[15] C.R. Dickson and R.N. Zare, Chem. Phys. 7 (1975) 361.

[16] C.R. Dickson, J.B. Kinney and R.N. Zare, Chem. Phys. 15 (1976) 243.

[17] U. Brinkmann, A. Steudel and H. Walther, Z. Angew. Phys. 22 (1967) 223.

[18] S. Ishii and W. Ohlendorf, Rev. Sci. Instr. 43 (1972) 1632.

[19] S.M. Heider and G.O. Brink, Rev. Sci. Instr. 46 (1975) 488.

[20] B.G. Wicke, M.A. Revelli and D.O. Harris, J. Chem. Phys. 63 (1975) 3120.
[21] D.V. Geppert, Basic electron tubes (McGraw–Hill, New York, 1951) pp. 223–228.
[22] S. Trajmar, J.K. Rice and A. Kupperman, Advan. in Chem. Phys. 18 (1970) 15.
[23] S.G. Schmelling, Phys. Rev. A9 (1974) 1097.
[24] P.J. Dagdigian, H.W. Cruse and R.N. Zare, J. Chem. Phys. 60 (1974) 2330.
[25] L. Pasternack and P.J. Dagdigian, to be published.
[26] C.D. Jonah and R.N. Zare, Chem. Phys. Letters 9 (1971) 65.
[27] D.J. Wren and M. Menzinger, Chem. Phys. Letters 27 (1974) 572.
[28] C.A. Mims and J.H. Brophy, J. Chem. Phys. 66 (1977) 1378.
[29] M.M. Patel and N.R. Shah, Indian J. Pure Appl. Phys. 8 (1970) 681.
[30] D.R. Preuss and J.L. Gole, J. Chem. Phys. 66 (1977) 2994.
[31] R.C. Estler and R.N. Zare, unpublished work.
[32] L. Pasternack and P.J. Dagdigian, Rev. Sci. Instr. 48 (1977) 226.
[33] C.E. Moore, Atomic energy levels (National Bureau of Standard, 1958) pp. 131–133.
[34] D.R. Herschbach, Advan. Chem. Phys. 10 (1966) 319.
[35] S. Datz and R.E. Minturn, J. Chem. Phys. 41 (1964) 1153;
R.R. Herm, R. Gordon and D.R. Herschbach, J. Chem. Phys. 41 (1964) 2218;
J.R. Wilson, G.H. Kwei, J.A. Norris, R.R. Herm, J.H. Birely and D.R. Herschbach, J. Chem. Phys. 41 (1964) 1154;
A.E. Grosser and R.B. Bernstein, J. Chem. Phys. 43 (1965) 1140;
R.R. Herm and D.R. Herschbach, J. Chem. Phys. 43 (1965) 2139;
J.H. Birely and D.R. Herschbach, J. Chem. Phys. 44 (1966) 1690;
D.R. Herschbach, Appl. Optics, Suppl. 2 (Chemical Lasers) (1965) 128.
[36] J.J. DeCorpo and J.L. Franklin, J. Chem. Phys. 54 (1971) 1885.
[37] O.F. Hagena and A.K. Varma, Rev. Sci. Instr. 39 (1967) 47;
J.A. Alcalay and E.L. Knuth, Rev. Sci. Instr. 40 (1969) 438;
O.F. Hagena, Rev. Sci. Instr. 41 (1970) 893;
J.A. Alcalay and E.L. Knuth, Rev. Sci. Instr. 4 (1971) 399;
W.S. Young, Rev. Sci. Instr. 44 (1973) 715;
P.B. Scott, P.H. Bauer, H.Y. Wachman and L. Trilling, Rarefied gas dynamics, Vol. 2, Suppl. 4, ed. A. Brundin (Academic, New York, 1967) pp. 1353–1368.
[38] T.D. Gaily, S.D. Rosner and R.A. Holt, Rev. Sci. Instr. 47 (1976) 143.
[39] M. Menzinger, Can. J. Chem. 52 (1974) 1688.
[40] J.C. Polanyi, Appl. Optics, Suppl. 2 (Chemical Lasers) (1965) 109.
[41] P.J. Dagdigian, H.W. Cruse and R.N. Zare, J. Chem. Phys. 62 (1975) 1824.
[42] D.L. Hildenbrand, J. Chem. Phys. 66 (1977) 3526.
[43] D.L. Hildenbrand, submitted for publication in J. Chem. Phys..
[44] I.S. Gradshteyn and I.M. Ryzhik, Tables of integrals, series, and products (Academic Press, New York, 1965) p. 338, eq. 3.462.5.
[45] K.S. Krasnov and N.V. Karaseva, Opt. Spectry. 19 (1965) 14.
[46] J.L. Gole, unpublished results, as reported in ref. [5].
[47] L.V. Gurvich, V.G. Ryabova and A.N. Khitrov, Faraday Symp. Chem. Soc. 8 (1973) 83.
[48] R.F. Barrow, D.F. Broyd, L.B. Pederson and K.K. Yee, Chem. Phys. Letters 18 (1973) 357.
[49] R.F. Barrow and K.K. Yee, Faraday Trans. II 69 (1973) 684.
[50] J.A. Horsley and R.F. Barrow, Trans. Faraday Soc. 63 (1967) 32.